A $\{Cu_2I_3^-\}_\infty$ chain hybrid with two-step phase transition, switchable dielectrics, reversible thermochromism and irreversible piezochromism

Qing-Qing Li,[#a] Xue-Wei Pan,[#a] Jin Zhang,*[a] Lu Zhai,[a] Xiao-Ming Ren*[a, b, c]

[a] State Key Laboratory of Materials-Oriented Chemical Engineering and College of Chemistry and Molecular Engineering, Nanjing Tech University, Nanjing 211816, P. R. China

[b] College of Materials Science and Engineering, Nanjing Tech University, Nanjing 211816, P. R. China

[c] State Key Laboratory of Coordination Chemistry, Nanjing University, Nanjing 210093, P. R. China

[#] These authors contribute equally to this work

Tel: 86-25-58139476

E-mail: 1084752558@qq.com (JZ)

xmren@njtech.edu.cn (XMR)

Contents

Table S1: Crystallographic data and refinement parameters of **1** at 223, 298, 360 and 400 K

Temp. / K	223	298
Chemical formula	$C_5H_{14}NCu_2I_3$	$C_5H_{14}NCu_2I_3$
CCDC number	2216272	2216273
Formula weight	595.95	595.95
Crystal system	Triclinic	Triclinic
Space group	*P-1*	*P-1*
a / Å	8.2892(3)	8.3083(6)
b / Å	9.5653(3)	9.6704(7)
c / Å	9.7954(3)	9.9142(6)
α / °	61.1868(9)	60.925(2)
β / °	83.7127(11)	83.001(2)
γ / °	85.3326(11)	85.120(2)
V ($Å^3$) / Z	676.05(4)	690.68(8)
Calc.density g/cm	7.478	2.866
Abs.coeff. μ/mms	26.800	9.740
F(000)	1344	536
θ range for data collection /°	2.47 to 26.39	2.36 to 24.99
Index range	$-10 \le h \le 10$	$-9 \le h \le 9$
	$-9 \le k \le 11$	$-11 \le k \le 11$
	$0 \le l \le 12s$	$-11 \le l \le 11$
Refl. collected/unique	2725/2725	14013/2428
R_{int}	0.0365	0.0770
Goodness-of-fit on F^2	1.069	1.088
Final R indices [I>2σ(I)]	$R_1 = 0.0467$	$R_1 = 0.0792$
	$wR_2 = 0.1147$	$wR_2 = 0.2173$
R indices(all data)	$R_1 = 0.0603$	$R_1 = 0.0842$
	$wR_2 = 0.1271$	$wR_2 = 0.2238$
Residual(e $Å^{-3}$)	1.384/−1.610	1.560/−2.432

Continue to Table 1

Temp. / K	360	400
Chemical formula	$C_5H_{14}NCu_2I_3$	$C_5H_{14}NCu_2I_3$
CCDC number	2216274	2216275
Formula weight	595.95	595.95
Crystal system	Monoclinic	Monoclinic
Space group	*P21/n*	*P21/n*
a / Å	8.3123(6)	8.3199(8)
b / Å	17.2607(14)	17.3332(17)
c / Å	9.8344(8)	9.8770(10)
α / °	90	90.00
β / °	94.641(2)	94.569(3)
γ / °	90	90.00
V ($Å^3$) / Z	1406.37(19)	1419.8(2)
Calc.density g/cm	2.815	2.788
Abs.coeff. μ/mms	9.567	9.476
F(000)	1072	1072
θ range for data collection /°	2.73 to 26.37	2.72 to 26.44
Index range	$-9 \le h \le 10$	$-9 \le h \le 10$
	$-20 \le k \le 21$	$-20 \le k \le 21$
	$-12 \le l \le 12$	$-12 \le l \le 12$
Refl. collected/unique	10245/2855	11647/2893
R_{int}	0.0395	0.0355
Goodness-of-fit on F^2	1.063	1.055
Final R indices [I>2σ(I)]	$R_1 = 0.0586$	$R_1 = 0.0543$
	$wR_2 = 0.1535$	$wR_2 = 0.1435$
R indices(all data)	$R_1 = 0.0911$	$R_1 = 0.0892$
	$wR_2 = 0.1779$	$wR_2 = 0.1700$
Residual(e $Å^{-3}$)	1.870/–0.872	1.395/–0.745

Table S2: Bond lengths (Å) in $\{Cu_2I_3^-\}_\infty$ chain in crystal structures of **1** at 223, 298, 360 and 400 K

T = 223 K		T = 298 K	
Atom pair	Distance / Å	Atom pair	Distance / Å
Cu(1)-I(3)	2.535(2)	I(1)-Cu(2)	2.533(2)
Cu(1)-I(2)	2.645(2)	I(1)-Cu(1)$^{\#1}$	2.781(3)
Cu(1)-Cu(1)$^{\#1}$	2.651(4)	I(1)-Cu(2)$^{\#1}$	2.847(3)
Cu(1)-I(1)	2.744(2)	I(3)-Cu(1)	2.532(2)
Cu(1)-I(3)$^{\#1}$	2.842(2)	I(3)-Cu(2)$^{\#2}$	2.763(3)
Cu(2)-I(1)$^{\#2}$	2.531(2)	I(3)-Cu(1)$^{\#2}$	2.875(3)
Cu(2)-I(2)	2.639(2)	I(2)-Cu(1)	2.636(3)
Cu(2)-Cu(2)$^{\#2}$	2.642(4)	I(2)-Cu(2)	2.644(3)
Cu(1)-Cu(2)	2.472(4)	Cu(2)-Cu(1)	2.464(3)
Cu(2)-I(3)$^{\#1}$	2.767(2)	Cu(2)-Cu(2)$^{\#1}$	2.674(6)
Cu(2)-I(1)	2.871(2)	Cu(2)-I(3)$^{\#2}$	2.763(3)
I(1)-Cu(2)$^{\#2}$	2.531(2)	Cu(2)-I(1)$^{\#1}$	2.847(3)
I(3)-Cu(2)$^{\#1}$	2.767(2)	Cu(1)-Cu(1)$^{\#2}$	2.663(6)
I(3)-Cu(1)$^{\#1}$	2.842(2)	Cu(1)-I(1)$^{\#1}$	2.781(3)
		Cu(1)-I(3)$^{\#2}$	2.875(3)

Symmetry codes:

T = 223 K: #1 = -x+2, -y, -z+1, #2 = -x+1, -y, -z+1

T = 298 K: #1 = -x+2, -y+1, -z+2; #2 = -x+1, -y+1, -z+2

Continue to Table 2

T = 360 K		T = 400 K	
Atom pair	Distance / Å	Atom pair	Distance / Å
Cu(1)-I(3)	2.524(2)	I(3)-Cu(1)	2.523(2)
Cu(1)-I(2)	2.634(3)	I(3)-Cu(2)	2.809(3)
Cu(1)-Cu(1)$^{\#1}$	2.684(5)	I(3)-Cu(1)$^{\#1}$	2.864(3)
Cu(1)-I(1)	2.802(3)	I(2)-Cu(2)	2.628(2)
Cu(1)-I(3)$^{\#1}$	2.873(3)	I(2)-Cu(1)$^{\#1}$	2.637(2)
Cu(2)-I(1)$^{\#2}$	2.526(2)	I(1)-Cu(2)	2.522(2)
Cu(2)-I(2)	2.640(2)	I(1)-Cu(1)$^{\#2}$	2.800(3)
Cu(2)-Cu(2)$^{\#2}$	2.691(5)	I(1)-Cu(2)$^{\#3}$	2.877(3)
Cu(1)-Cu(2)	2.464(5)	Cu(2)-Cu(1)$^{\#1}$	2.461(3)
Cu(2)-I(3)$^{\#1}$	2.794(3)	Cu(2)-Cu(2)$^{\#3}$	2.701(5)
Cu(2)-I(1)	2.856(3)	Cu(2)-I(1)$^{\#3}$	2.877(3)
I(1)-Cu(2)$^{\#2}$	2.526(2)	Cu(1)-Cu(2)$^{\#1}$	2.461(3)
I(3)-Cu(2)$^{\#1}$	2.794(3)	Cu(1)-I(2)$^{\#1}$	2.637(2)
I(3)-Cu(1)$^{\#1}$	2.873(3)	Cu(1)-Cu(1)$^{\#1}$	2.704(5)
		Cu(1)-I(1)$^{\#4}$	2.800(3)
		Cu(1)-I(3)$^{\#1}$	2.864(3)

Symmetry codes:

T = 360 K: #1 = -x+1, -y+1, -z+1; #2 = -x+2, -y+1, -z+1

T = 400 K: #1 = -x+2, -y+1, -z+1; #2 = x-1, y, z; #3 = -x+1, -y+1, -z+1; #4 = x+1, y, z

Table S3: Bond lengths (Å) in $C_5H_{14}N^+$ cation in crystal structures of **1** at 223, 298, 360 and 400 K

T = 223 K		T = 298 K	
Atom pair	Distance / Å	Atom pair	Distance / Å
N(1)-C(4)	1.36(2)	N(1)-C(5)	1.424(18)
N(1)-C(3)	1.462(19)	N(1)-C(1)	1.423(17)
N(1)-C(1)	1.496(17)	N(1)-C(2)	1.421(17)
N(1)-C(2)	1.62(3)	N(1)-C(3)	1.454(17)
C(5)-C(4)	1.69(4)	C(5)-C(4)	1.488(17)

Symmetry codes:

T = 223 K: #1 = -x+2, -y, -z+1; #2 = -x+1, -y, -z+1

T = 298 K: #1 = -x+2, -y+1, -z+2; #2 = -x+1, -y+1, -z+2

Continue to Table 3

T = 360 K		T = 400 K	
Atom pair	Distance / Å	Atom pair	Distance / Å
N(1)-C(3)	1.408(18)	N(1)-C(3)	1.403(17)
N(1)-C(1)	1.432(18)	N(1)-C(5)	1.457(17)
N(1)-C(4)	1.441(18)	N(1)-C(1)	1.429(17)
N(1)-C(2)	1.468(18)	N(1)-C(2)	1.450(17)
C(4)-C(5)	1.581(10)	C(4)-C(5)	1.458(18)

Symmetry codes:

T = 360 K: #1 = -x+1, -y+1, -z+1; #2 = -x+2, -y+1, -z+1

T = 400 K: #1 = -x+2, -y+1, -z+1; #2 = x-1, y, z

Table S4: Bond angles (°) in $\{Cu_2I_3^-\}_\infty$ chain in crystal structures of **1** at 223, 298, 360 and 400 K

T = 223 K		T = 298 K	
Atoms	Angle / °	Atoms	Angle / °
I(3)-Cu(1)-I(2)	115.91(7)	Cu(2)-I(1)-Cu(1)$^{\#1}$	111.19(9)
I(3)-Cu(1)-Cu(1)$^{\#1}$	66.43(6)	Cu(2)-I(1)-Cu(2)$^{\#1}$	59.29(10)
I(2)-Cu(1)-Cu(1)$^{\#1}$	130.07(12)	Cu(1)$^{\#1}$-I(1)-Cu(2)$^{\#1}$	51.90(7)
I(3)-Cu(1)-I(1)	112.15(7)	Cu(1)-I(3)-Cu(2)$^{\#2}$	110.35(9)
I(2)-Cu(1)-I(1)	105.52(6)	Cu(1)-I(3)-Cu(1)$^{\#2}$	58.59(11)
Cu(1)$^{\#1}$-Cu(1)-I(1)	119.80(11)	Cu(2)$^{\#2}$-I(3)-Cu(1)$^{\#2}$	51.78(7)
I(3)-Cu(1)-I(3)$^{\#1}$	121.25(7)	Cu(1)-I(2)-Cu(2)	55.63(8)
I(2)-Cu(1)-I(3)$^{\#1}$	102.16(6)	Cu(1)-Cu(2)-I(1)	176.60(17)
Cu(1)$^{\#1}$-Cu(1)-I(3)$^{\#1}$	54.82(7)	Cu(1)-Cu(2)-I(2)	62.01(9)
I(1)-Cu(1)-I(3)$^{\#1}$	97.32(6)	I(1)-Cu(2)-I(2)	116.18(10)
I(1)$^{\#2}$-Cu(2)-I(2)	116.53(7)	Cu(1)-Cu(2)-Cu(2)$^{\#1}$	117.18(18)
I(1)$^{\#2}$-Cu(2)-Cu(2)$^{\#2}$	67.39(6)	I(1)-Cu(2)-Cu(2)$^{\#1}$	66.22(9)
I(2)-Cu(2)-Cu(2)$^{\#2}$	131.10(13)	I(2)-Cu(2)-Cu(2)$^{\#1}$	130.45(19)
I(1)$^{\#2}$-Cu(2)-I(3)$^{\#1}$	112.73(8)	Cu(1)-Cu(2)-I(3)$^{\#2}$	66.46(10)
I(2)-Cu(2)-I(3)$^{\#1}$	104.35(6)	I(1)-Cu(2)-I(3)$^{\#2}$	112.09(11)
Cu(2)$^{\#2}$-Cu(2)-I(3)$^{\#1}$	119.08(11)	I(2)-Cu(2)-I(3)$^{\#2}$	105.38(9)
I(1)$^{\#2}$-Cu(2)-I(1)	121.86(7)	Cu(2)$^{\#1}$-Cu(2)-I(3)$^{\#2}$	119.57(16)
I(2)-Cu(2)-I(1)	102.19(7)	Cu(1)-Cu(2)-I(1)$^{\#1}$	62.68(10)
Cu(2)$^{\#2}$-Cu(2)-I(1)	54.47(7)	I(1)-Cu(2)-I(1)$^{\#1}$	120.71(10)
I(3)$^{\#1}$-Cu(2)-I(1)	96.12(6)	I(2)-Cu(2)-I(1)$^{\#1}$	102.53(9)
Cu(2)$^{\#2}$-I(1)-Cu(1)	110.31(6)	Cu(2)$^{\#1}$-Cu(2)-I(1)$^{\#1}$	54.50(10)
Cu(2)$^{\#2}$-I(1)-Cu(2)	58.14(7)	I(3)$^{\#2}$-Cu(2)-I(1)$^{\#1}$	97.42(9)
Cu(1)-I(1)-Cu(2)	52.18(5)	Cu(2)-Cu(1)-I(3)	176.60(18)
Cu(2)-I(2)-Cu(1)	55.78(5)	Cu(2)-Cu(1)-I(2)	62.37(9)
Cu(1)-I(3)-Cu(2)$^{\#1}$	111.02(6)	I(3)-Cu(1)-I(2)	116.80(11)
Cu(1)-I(3)-Cu(1)$^{\#1}$	58.75(7)	Cu(2)-Cu(1)-Cu(1)$^{\#2}$	116.00(18)
Cu(2)$^{\#1}$-I(3)-Cu(1)$^{\#1}$	52.27(5)	I(3)-Cu(1)-Cu(1)$^{\#2}$	67.16(9)
		I(2)-Cu(1)-Cu(1)$^{\#2}$	131.5(2)
		Cu(2)-Cu(1)-I(1)$^{\#1}$	65.41(10)
		I(3)-Cu(1)-I(1)$^{\#1}$	112.24(12)
		I(2)-Cu(1)-I(1)$^{\#1}$	104.54(9)
		Cu(1)$^{\#2}$-Cu(1)-I(1)$^{\#1}$	118.63(16)
		Cu(2)-Cu(1)-I(3)$^{\#2}$	61.76(10)
		I(3)-Cu(1)-I(3)$^{\#2}$	121.41(11)
		I(2)-Cu(1)-I(3)$^{\#2}$	102.54(10)
		Cu(1)$^{\#2}$-Cu(1)-I(3)$^{\#2}$	54.26(10)
		I(1)$^{\#1}$-Cu(1)-I(3)$^{\#2}$	96.34(8)

Symmetry codes:

T = 223 K: #1 = -x+2, -y, -z+1; #2 = -x+1, -y, -z+1

T = 298 K: #1 = -x+2, -y+1, -z+2； #2 = -x+1, -y+1, -z+2

Continue to Table S4

T = 360 K		T = 400 K	
Atoms	Angle / °	Atoms	Angle / °
I(3)-Cu(1)-I(2)	117.73(9)	Cu(2)-I(1)-Cu(1)	111.25(8)
I(3)-Cu(1)-Cu(1)$^{\#1}$	66.88(8)	Cu(2)-I(1)-Cu(2)$^{\#1}$	59.85(9)
I(2)-Cu(1)-Cu(1)$^{\#1}$	132.33(17)	Cu(1)-I(1)-Cu(2)$^{\#1}$	51.41(6)
I(3)-Cu(1)-I(1)	111.20(10)	Cu(1)-I(2)-Cu(2)$^{\#1}$	55.74(7)
I(2)-Cu(1)-I(1)	104.96(8)	Cu(1)-I(3)-Cu(2)$^{\#2}$	110.93(8)
Cu(1)$^{\#1}$-Cu(1)-I(1)	117.43(14)	Cu(1)-I(3)-Cu(1)$^{\#3}$	59.61(9)
I(3)-Cu(1)-I(3)$^{\#1}$	120.79(9)	Cu(2)$^{\#2}$-I(3)-Cu(1)$^{\#3}$	51.36(6)
I(2)-Cu(1)-I(3)$^{\#1}$	102.72(9)	Cu(2)$^{\#1}$-Cu(1)-I(3)	176.14(15)
Cu(1)$^{\#1}$-Cu(1)-I(3)$^{\#1}$	53.91(9)	Cu(2)$^{\#1}$-Cu(1)-I(2)	62.32(7)
I(1)-Cu(1)-I(3)$^{\#1}$	96.46(7)	I(3)-Cu(1)-I(2)	117.74(9)
I(1)$^{\#2}$-Cu(2)-I(2)	117.24(10)	Cu(2)$^{\#1}$-Cu(1)-Cu(1)$^{\#3}$	116.33(15)
I(1)$^{\#2}$-Cu(2)-Cu(2)$^{\#2}$	66.30(8)	I(3)-Cu(1)-Cu(1)$^{\#3}$	66.73(7)
I(2)-Cu(2)-Cu(2)$^{\#2}$	132.35(16)	I(2)-Cu(1)-Cu(1)$^{\#3}$	132.43(17)
I(1)$^{\#2}$-Cu(2)-I(3)$^{\#1}$	111.37(10)	Cu(2)$^{\#1}$-Cu(1)-I(1)	65.46(8)
I(2)-Cu(2)-I(3)$^{\#1}$	104.74(8)	I(3)-Cu(1)-I(1)	111.26(10)
Cu(2)$^{\#2}$-Cu(2)-I(3)$^{\#1}$	118.16(14)	I(2)-Cu(1)-I(1)	105.12(8)
I(1)$^{\#2}$-Cu(2)-I(1)	120.38(9)	Cu(1)$^{\#3}$-Cu(1)-I(1)	117.18(13)
I(2)-Cu(2)-I(1)	103.30(8)	Cu(2)$^{\#1}$-Cu(1)-I(3)$^{\#3}$	62.72(8)
Cu(2)$^{\#2}$-Cu(2)-I(1)	54.07(9)	I(3)-Cu(1)-I(3)$^{\#3}$	120.39(9)
I(3)$^{\#1}$-Cu(2)-I(1)	97.03(8)	I(2)-Cu(1)-I(3)$^{\#3}$	103.03(9)
Cu(2)$^{\#2}$-I(1)-Cu(1)	111.23(8)	Cu(1)$^{\#3}$-Cu(1)-I(3)$^{\#3}$	53.65(9)
Cu(2)$^{\#2}$-I(1)-Cu(2)	59.62(9)	I(1)-Cu(1)-I(3)$^{\#3}$	96.37(7)
Cu(1)-I(1)-Cu(2)	51.62(6)	Cu(1)$^{\#1}$-Cu(2)-I(1)	176.42(15)
Cu(1)-I(2)-Cu(2)	55.70(7)	Cu(1)$^{\#1}$-Cu(2)-I(2)$^{\#1}$	61.94(7)
Cu(1)-I(3)-Cu(2)$^{\#1}$	110.69(8)	I(1)-Cu(2)-I(2)$^{\#1}$	117.33(9)
Cu(1)-I(3)-Cu(1)$^{\#1}$	59.21(9)	Cu(1)$^{\#1}$-Cu(2)-Cu(2)$^{\#1}$	116.90(15)
Cu(2)$^{\#1}$-I(3)-Cu(1)$^{\#1}$	51.52(6)	I(1)-Cu(2)-Cu(2)$^{\#1}$	66.35(7)
I(3)-Cu(1)-I(2)	117.73(9)	I(2)$^{\#1}$-Cu(2)-Cu(2)$^{\#1}$	132.28(16)
I(3)-Cu(1)-Cu(1)$^{\#1}$	66.88(8)	Cu(1)$^{\#1}$-Cu(2)-I(3)$^{\#4}$	65.92(8)
I(2)-Cu(1)-Cu(1)$^{\#1}$	132.33(17)	I(1)-Cu(2)-I(3)$^{\#4}$	111.51(9)
I(3)-Cu(1)-I(1)	111.20(10)	I(2)$^{\#1}$-Cu(2)-I(3)$^{\#4}$	104.88(8)
I(2)-Cu(1)-I(1)	104.96(8)	Cu(2)$^{\#1}$-Cu(2)-I(3)$^{\#4}$	117.92(13)
Cu(1)$^{\#1}$-Cu(1)-I(1)	117.43(14)	Cu(1)$^{\#1}$-Cu(2)-I(1)$^{\#1}$	63.12(9)
I(3)-Cu(1)-I(3)$^{\#1}$	120.79(9)	I(1)-Cu(2)-I(1)$^{\#1}$	120.15(9)
I(2)-Cu(1)-I(3)$^{\#1}$	102.72(9)	I(2)$^{\#1}$-Cu(2)-I(1)$^{\#1}$	103.34(8)
Cu(1)#1-Cu(1)-I(3)$^{\#1}$	53.91(9)	Cu(2)$^{\#1}$-Cu(2)-I(1)$^{\#1}$	53.80(9)
I(1)-Cu(1)-I(3)$^{\#1}$	96.46(7)	I(3)$^{\#4}$-Cu(2)-I(1)$^{\#1}$	96.84(7)

Symmetry codes:

T = 360 K: #1 = -x+1, -y+1, -z+1; #2 = -x+2, -y+1, -z+1

T = 400 K: #1 = -x+2, -y+1, -z+1; #2 = x-1, y, z; #3 = -x+1, -y+1, -z+1; #4 = x+1, y, z

Table S5: Bond angles (°) in $C_5H_{14}N^+$ cation in crystal structures of **1** at 223, 298, 360 and 400 K

T = 223 K		T = 298 K	
Atoms	Angle / °	Atoms	Angle / °
C(4)-N(1)-C(3)	118.7(18)	C(5)-N(1)-C(1)	110(2)
C(4)-N(1)-C(1)	118.5(15)	C(5)-N(1)-C(2)	117(2)
C(3)-N(1)-C(1)	112.6(12)	C(1)-N(1)-C(2)	115(2)
C(4)-N(1)-C(2)	94(2)	C(5)-N(1)-C(3)	99.1(15)
C(3)-N(1)-C(2)	102.9(19)	C(1)-N(1)-C(3)	109(3)
C(1)-N(1)-C(2)	105.0(15)	C(2)-N(1)-C(3)	106(2)
N(1)-C(4)-C(5)	98(2)	N(1)-C(5)-C(4)	100(3)

Symmetry codes:

T = 223 K: #1 = -x+2, -y, -z+1; #2 = -x+1, -y, -z+1

T = 298 K: #1 = -x+2, -y+1, -z+2; #2 = -x+1, -y+1, -z+2

Continue to Table S5

T = 360 K		T = 400 K	
Atoms	Angle / °	Atoms	Angle / °
C(3)-N(1)-C(1)	118(3)	C(3)-N(1)-C(5)	119(3)
C(3)-N(1)-C(4)	119(3)	C(3)-N(1)-C(1)	115(2)
C(1)-N(1)-C(4)	116(3)	C(5)-N(1)-C(1)	121(3)
C(3)-N(1)-C(2)	98(2)	C(3)-N(1)-C(2)	94(3)
C(1)-N(1)-C(2)	107(3)	C(5)-N(1)-C(2)	91.9(10)
C(4)-N(1)-C(2)	91.7(14)	C(1)-N(1)-C(2)	106(2)
N(1)-C(4)-C(5)	95(2)	N(1)-C(5)-C(4)	89(2)

Symmetry codes:

T = 360 K: #1 = -x+1, -y+1, -z+1; #2 = -x+2, -y+1, -z+1

T = 400 K: #1 = -x+2, -y+1, -z+1; #2 = x-1, y, z; #3 = -x+1, -y+1, -z+1; #4 = x+1, y, z

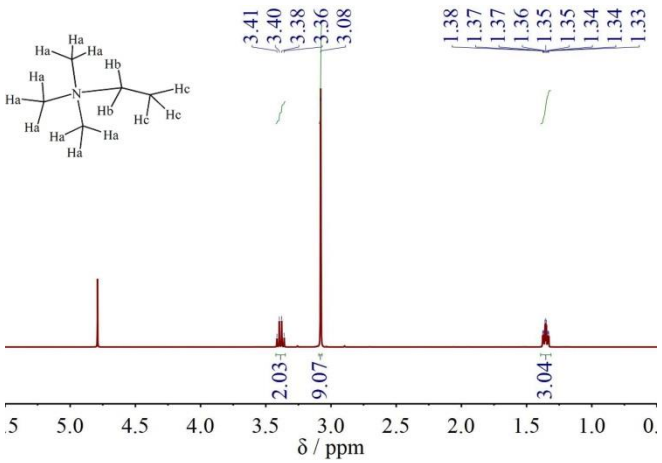

Fig. S1: The molecular structure of Me_3EtN^+ and ^1H NMR of $[Me_3EtN]Br$ (400 MHz, D_2O): 1.23–1.31 (3H, CH_3), 2.96–3.03 (9H, 3 CH_3), 3.26–3.34 (2H, CH_2), 4.96–4.72 (D_2O).

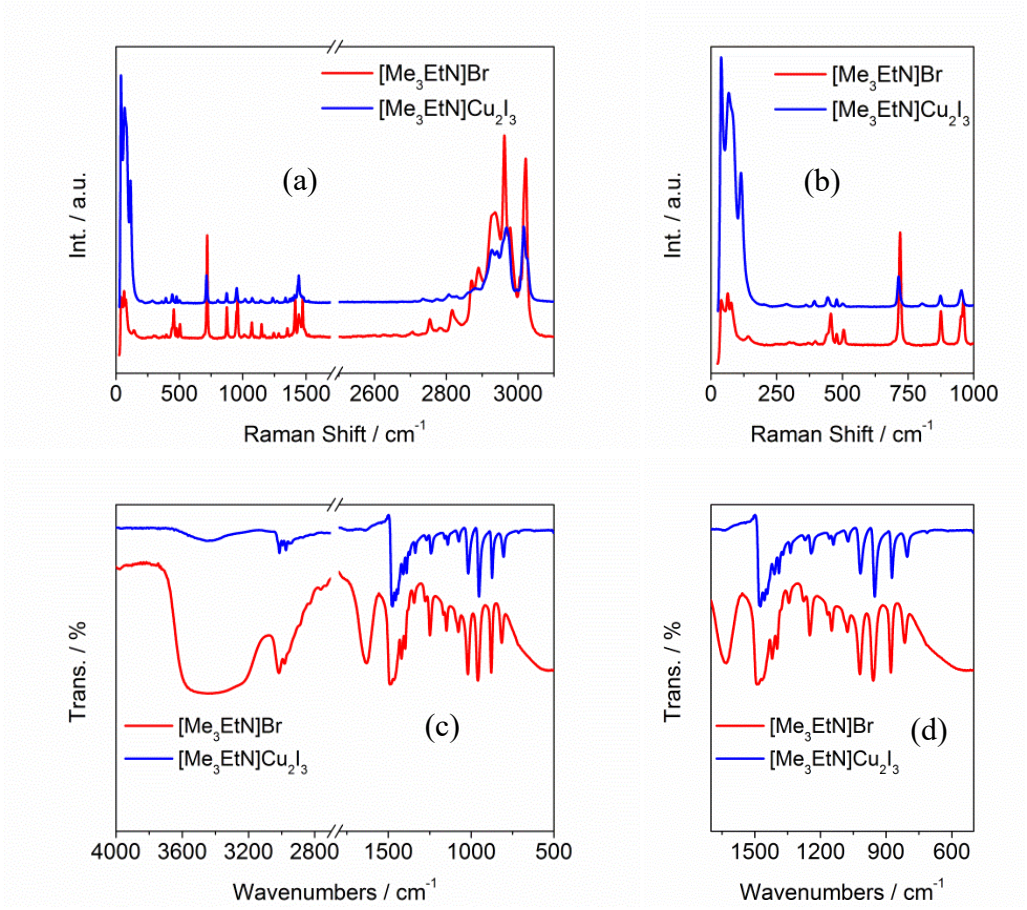

Fig. S2: Raman spectra of $[Me_3EtN]Br$ and **1** in the range of (a) 20–3100 cm^{-1} and (b) 20–1000 cm^{-1}. IR spectra of $[Me_3EtN]Br$ and **1** in the range of (c) 4000–500 cm^{-1} and (d) 1700–500 cm^{-1}.

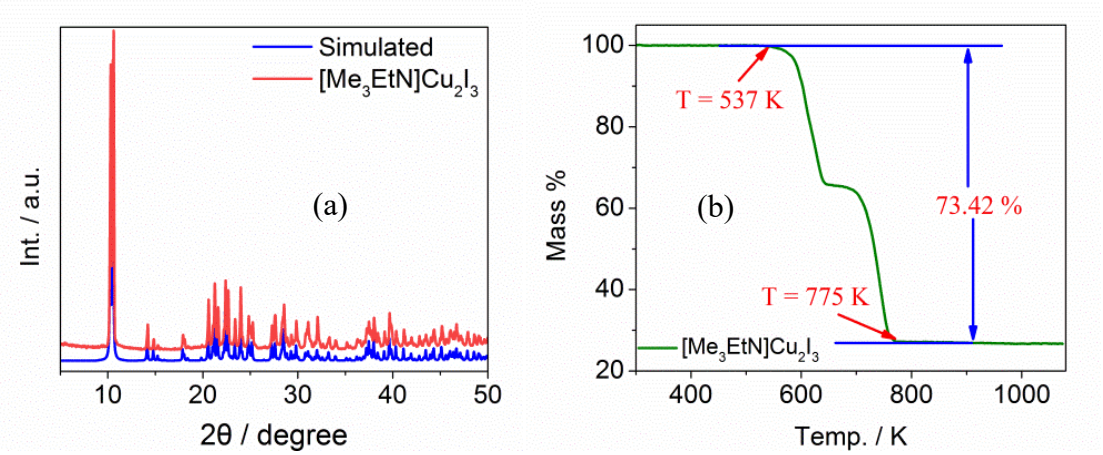

Fig. S3: (a) Experimental and simulated PXRD profiles at ambient condition and (b) TG plot of **1**, demonstrating that this hybrid is thermally stable below ca. 537 K, and then takes place two-step thermal decomposition, the weight loss of 36.0% between 537 and 699 K is in good agreement with the calculated value of 36.1%, corresponding to release completely Me_3EtI. The next weight loss is 36.75%, occurred between 699 and 776 K, and the detail is not clear for this process of decomposition at present stage.

Interestingly, **1** can be melted at *ca*. 513 K (Fig. S16), moreover, the melted liquid was also recrystallized when cooled down to ambient condition, and the recrystallized sample showed the same PXRD pattern as the pristine sample of **1**.

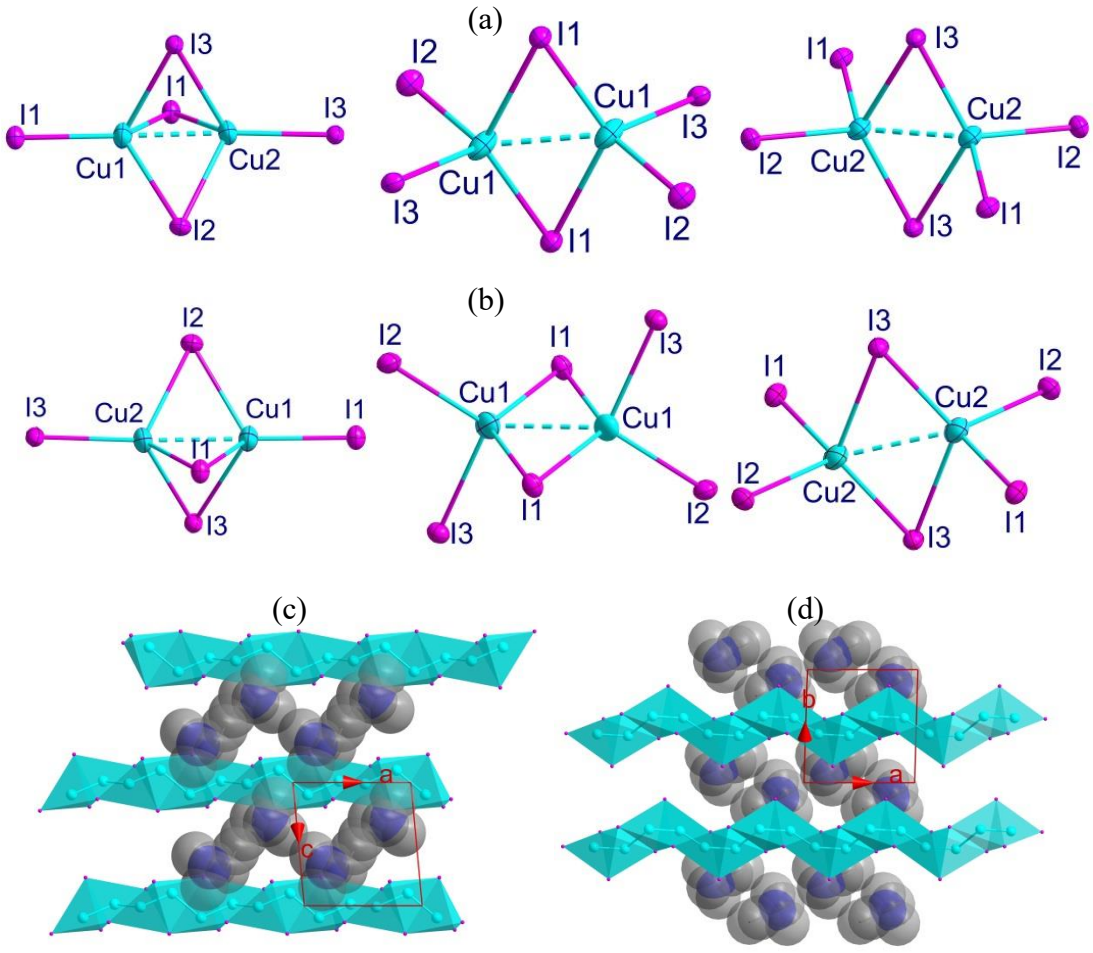

Fig. S4: Three different tetrahedral dimers at (a) 223 K, (b) 298 K and (c, d) packing diagrams viewed along *b*- and *c*-axis in the crystal structure of **1** at 223 K.

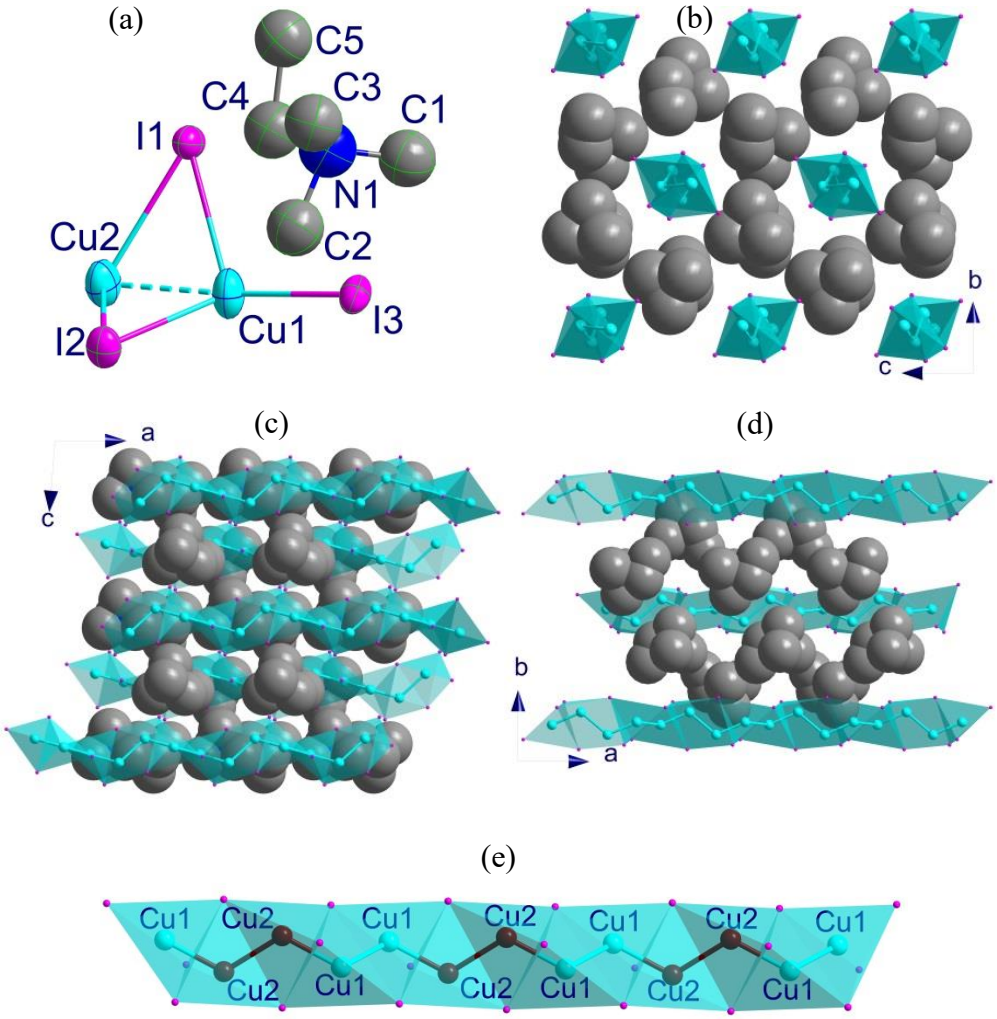

Fig. S5. (a) ORTEP view of **1** with thermal ellipsoid plot drawn at 20% probability level, (b–c) packing diagrams of **1** viewed along *a*-, *b*- and *c*-axes, respectively, (e) $\{Cu_2I_3^-\}_\infty$ chain in **1** at 360 K.

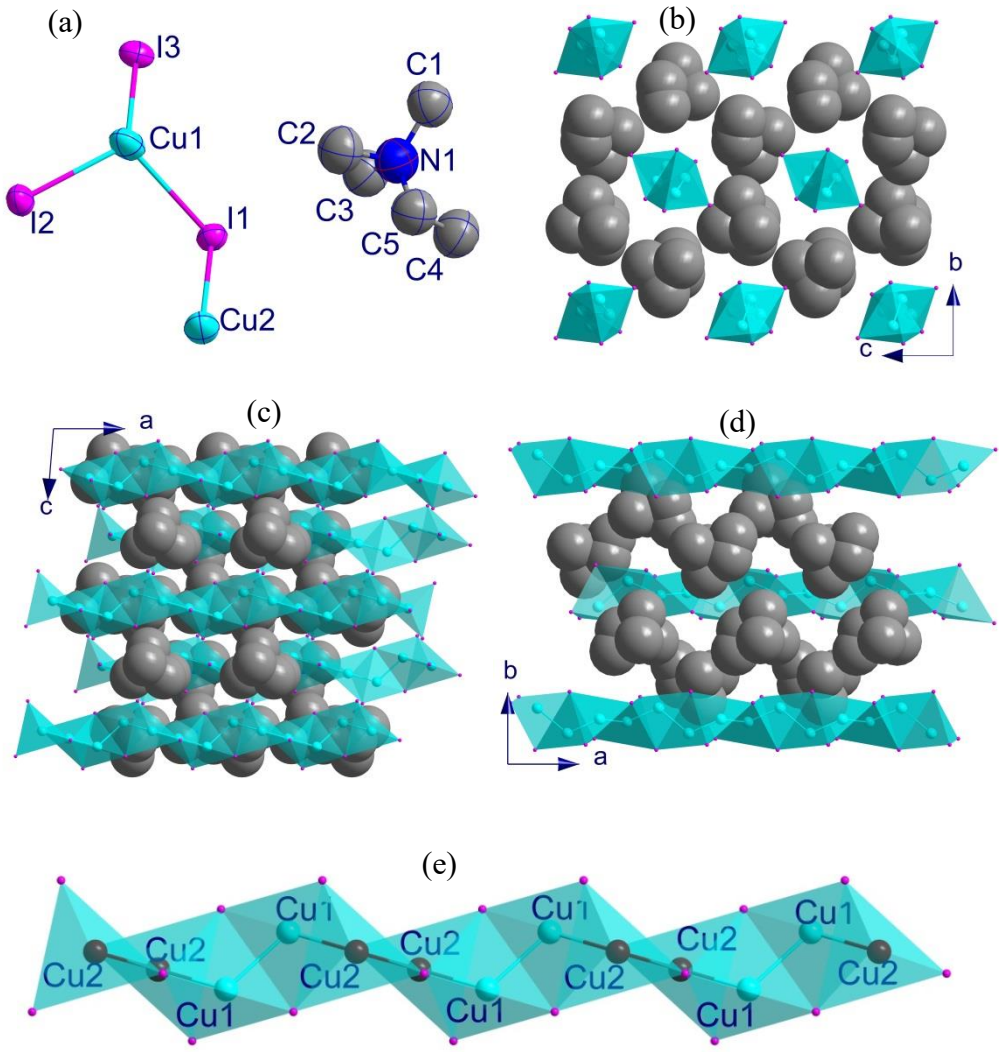

Fig. S6: (a) ORTEP view of **1** with thermal ellipsoid plot drawn at 20% probability level, (b–c) packing diagrams of **1** viewed along *a*-, *b*- and *c*-axes, respectively, (e) $\{Cu_2I_3^-\}_\infty$ chain in **1** at 400 K.

Cu1…Cu1dimer at 223 K

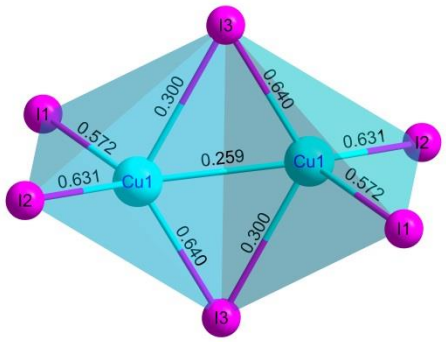

Cu1…Cu1dimer at 298 K

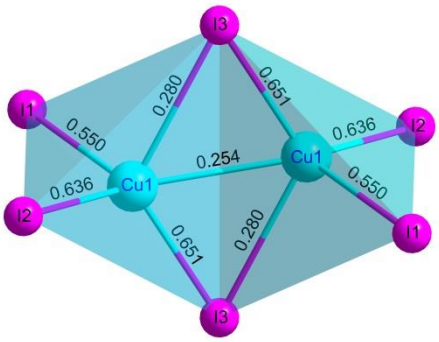

Cu1…Cu1dimer at 360 K

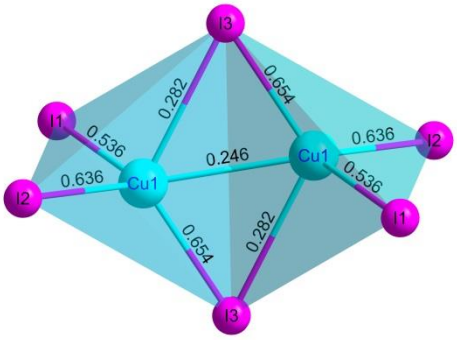

Cu1…Cu1dimer at 400 K

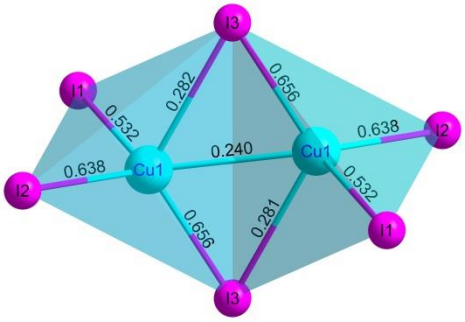

Cu1…Cu2 dimer at 223 K

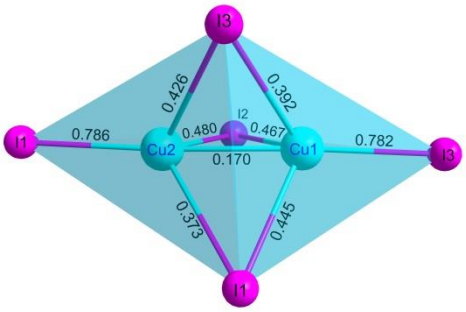

Cu1…Cu2 dimer at 298 K

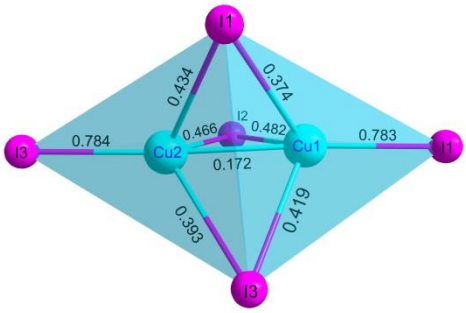

Cu1…Cu2 dimer at 360 K

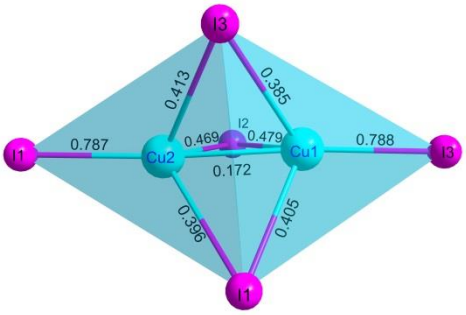

Cu1…Cu2 dimer at 400 K

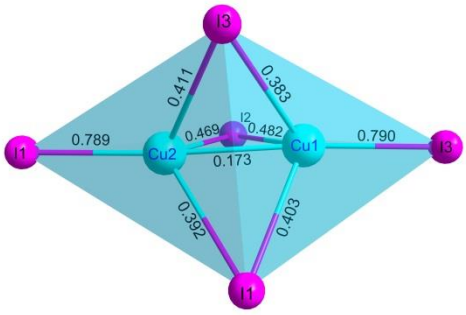

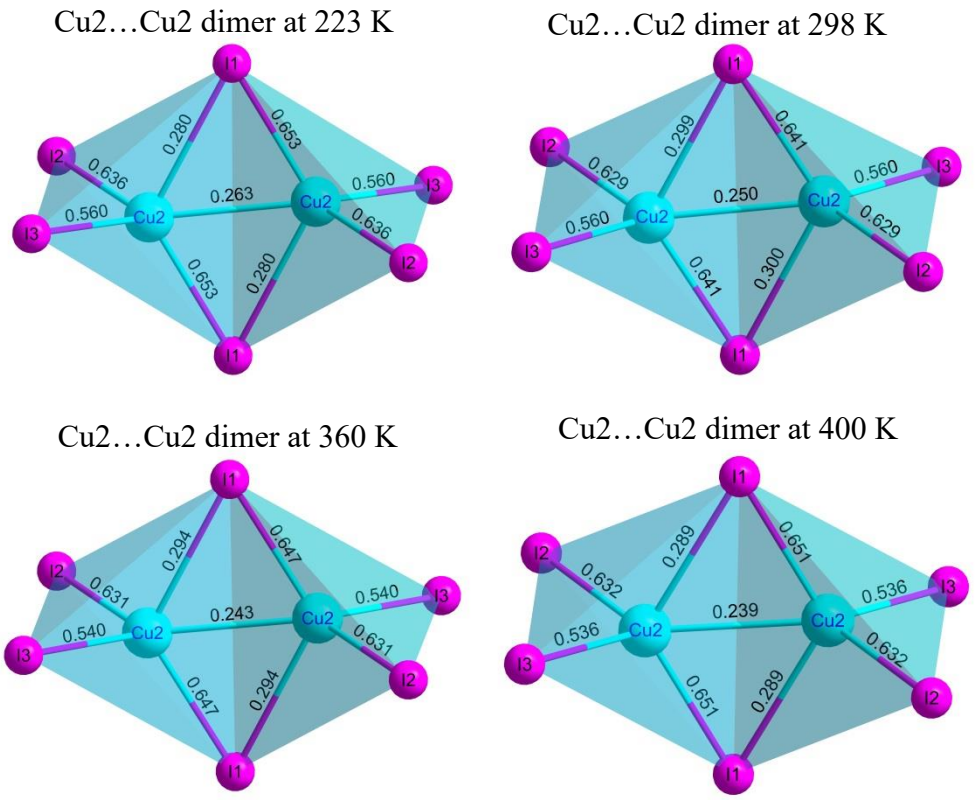

Fig. S7: Bond order analysis in a dimer of **1** with two face-sharing tetrahedra $[Cu_2I_5]^{3-}$ and two edge-sharing tetrahedra $[Cu_2I_6]^{4-}$ at 223, 298, 360 and 400 K.

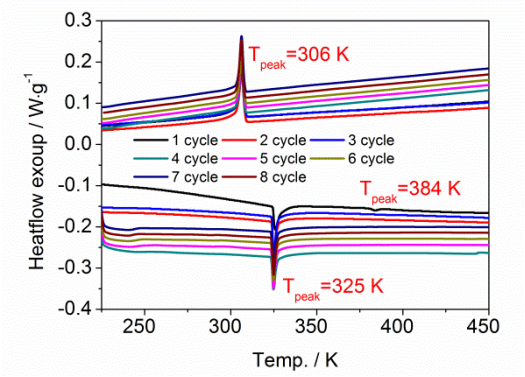

Fig. S8: DSC plots of **1**, in which the DSC measurements of **1** were carried out for three heating-cooling cycles (corresponding to the curves 1–3 cycles), and three months later, the DSC measurements were further performed for the same sample again, and the plots of five heating-cooling cycles are presented as the 4–cycle to 8–cycle, and these curves are almost the same as 2-cycle and 3-cycle.

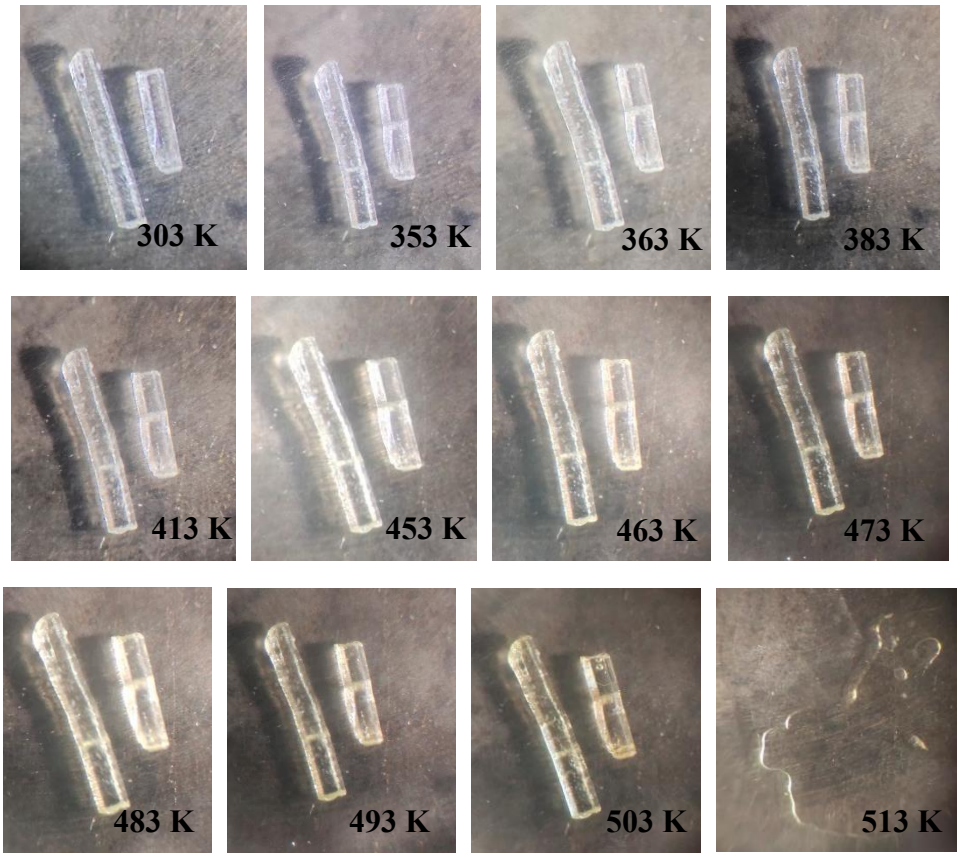

Fig. S9: Photos of crystal of **1** at 303–353 K (almost colorless), 363–463 K (light-yellow), 473–503 K (deeper light-yellow) and 513 K (melted). The pictures were taken by a Leica DMRX polarizing optical microscope equipped with an LINKAM LTS350 cool and hot stage.

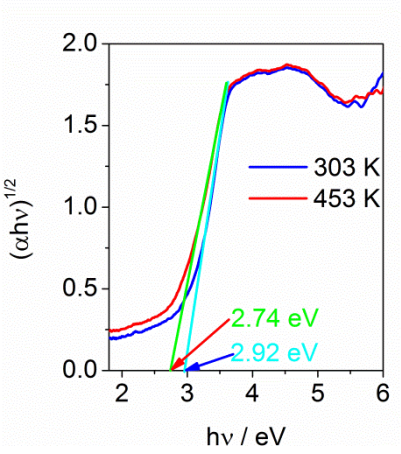

Fig. S10: Tauc plots of **1** at 303 and 453 K.

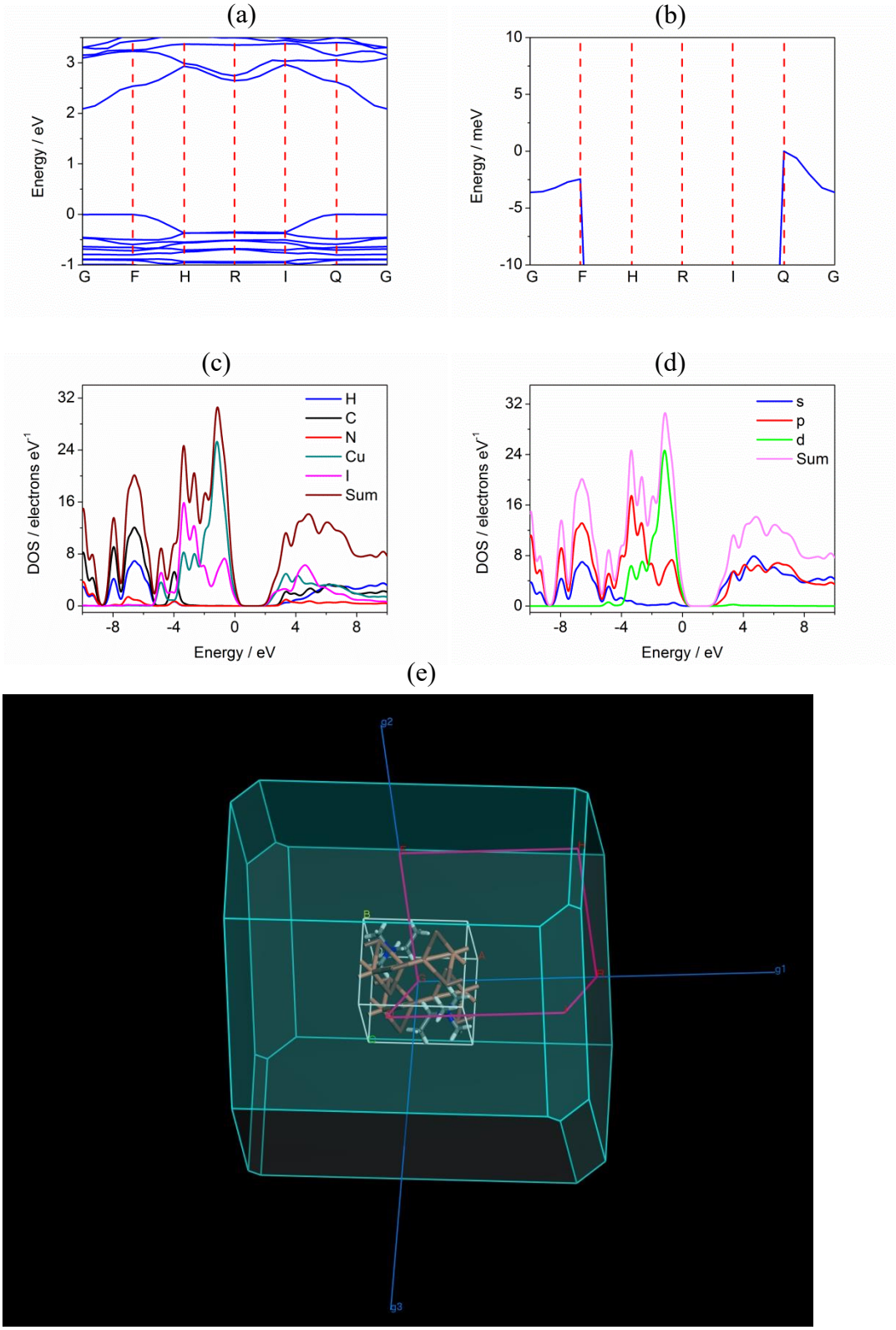

Fig. S11: (a, b) Energy band structures of **1** at 223 K. (c) Local density of states (LDOS), (d) projected density of states (PDOS) and (e) Brillouin zone in **1** at 223 K.

The bands exhibit a sharp dispersion along F → H and I → Q directions while a flat dispersion along other directions (Fig. S9e), demonstrating that there are stronger

orbital interactions along F → H and I → Q directions and weaker orbital interactions along G → F, G → Q, H → R and R → I directions. As shown in Fig. 4c, 4d and Fig. S9e, the directions F → H and I → Q are roughly parallel to the direction of $\{Cu_2I_3^-\}_\infty$ tetrahedral chains, and the directions G → F, G → Q, H → R and R → I are approximately perpendicular to the $\{Cu_2I_3^-\}_\infty$ tetrahedral chains, implying that there are stronger orbital interactions within $\{Cu_2I_3^-\}_\infty$ tetrahedral chains, whereas weaker intermolecular interactions between cations and $\{Cu_2I_3^-\}_\infty$ tetrahedral chains. This conclusion consists with the crystal structure analysis.

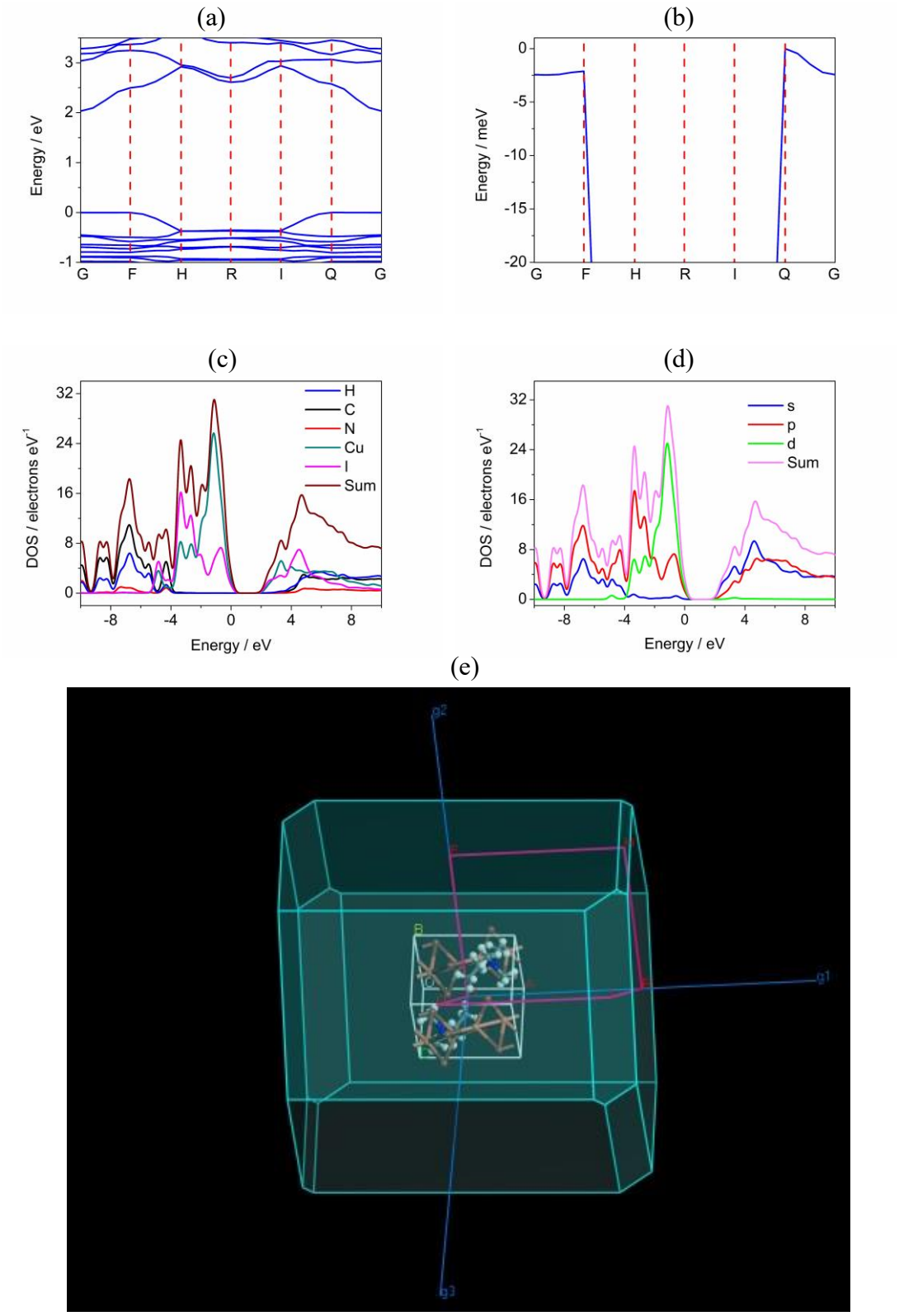

Fig. S12: (a, b) Energy band structures of **1** at 298 K. (c) Local density of states (LDOS), (d) projected density of states (PDOS) and (e) Brillouin zone in **1** at 298 K.

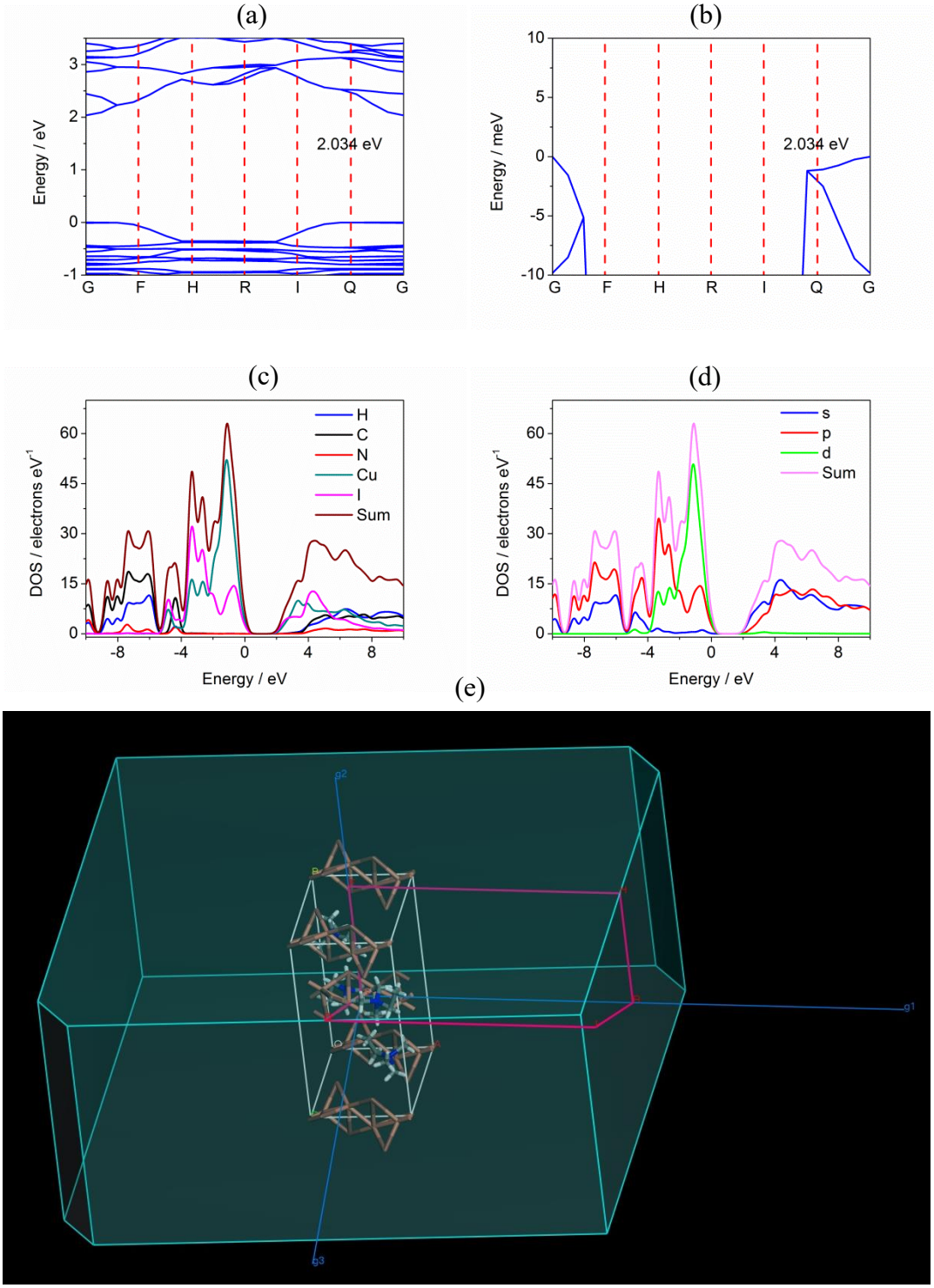

Fig. S13: (a, b) Energy band structures of **1** at 360 K. (c) Local density of states (LDOS), (d) projected density of states (PDOS) and (e) Brillouin zone in **1** at 360 K.

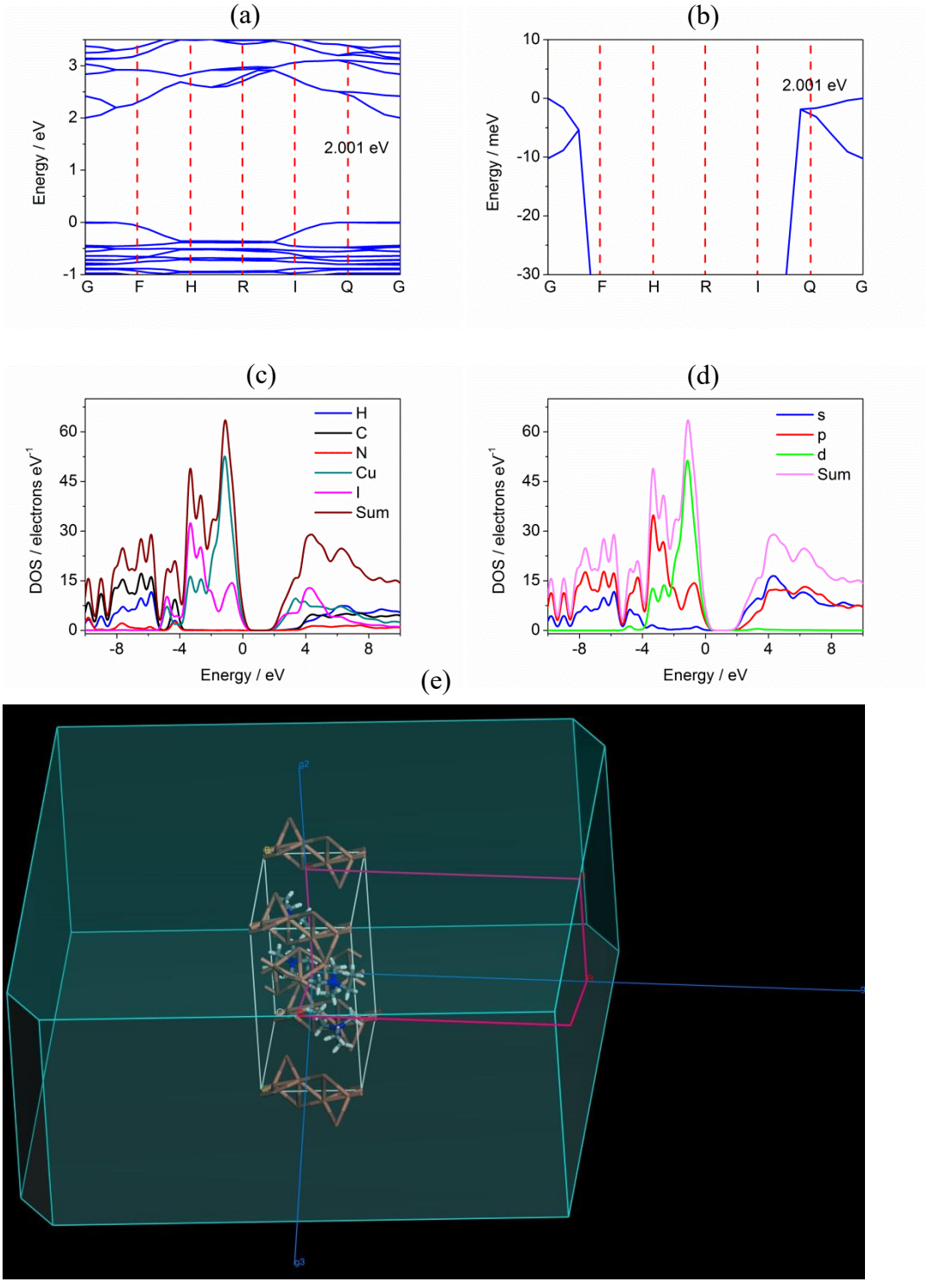

Fig. S14: (a, b) Energy band structures of **1** at 400 K. (c) Local density of states (LDOS), (d) projected density of states (PDOS) and (e) Brillouin zone in **1** at 400 K.

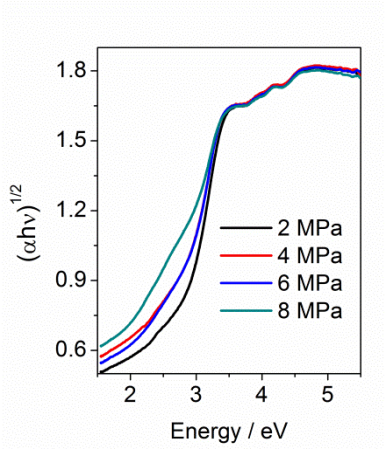

Fig. S14: Tauc plots of **1** transformed from solid diffuse UV-visible spectra under different pressures at room temperature.

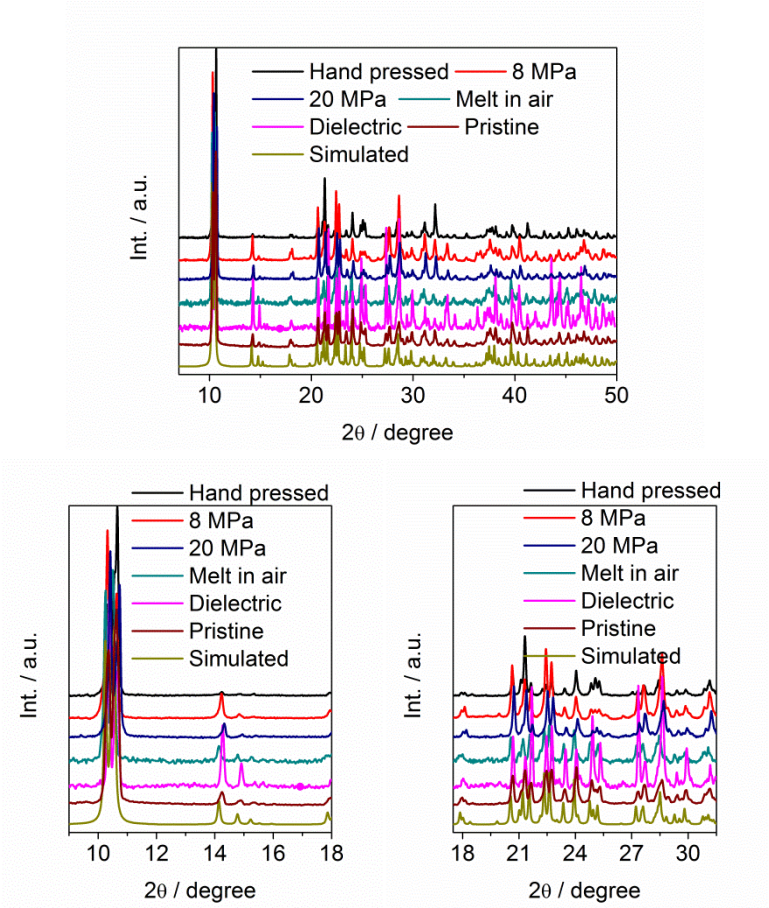

Fig. S15: PXRD patterns of **1** in which the samples were treated at different conditions in different 2θ regimes.

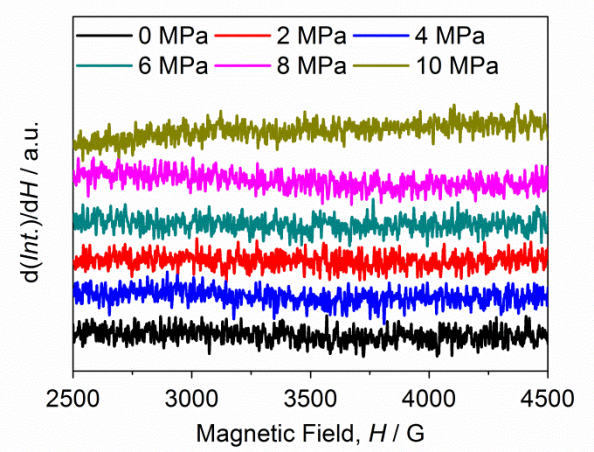

Fig. S16: EPR spectra of **1** where the samples were treated under different pressures recorded at room temperature.

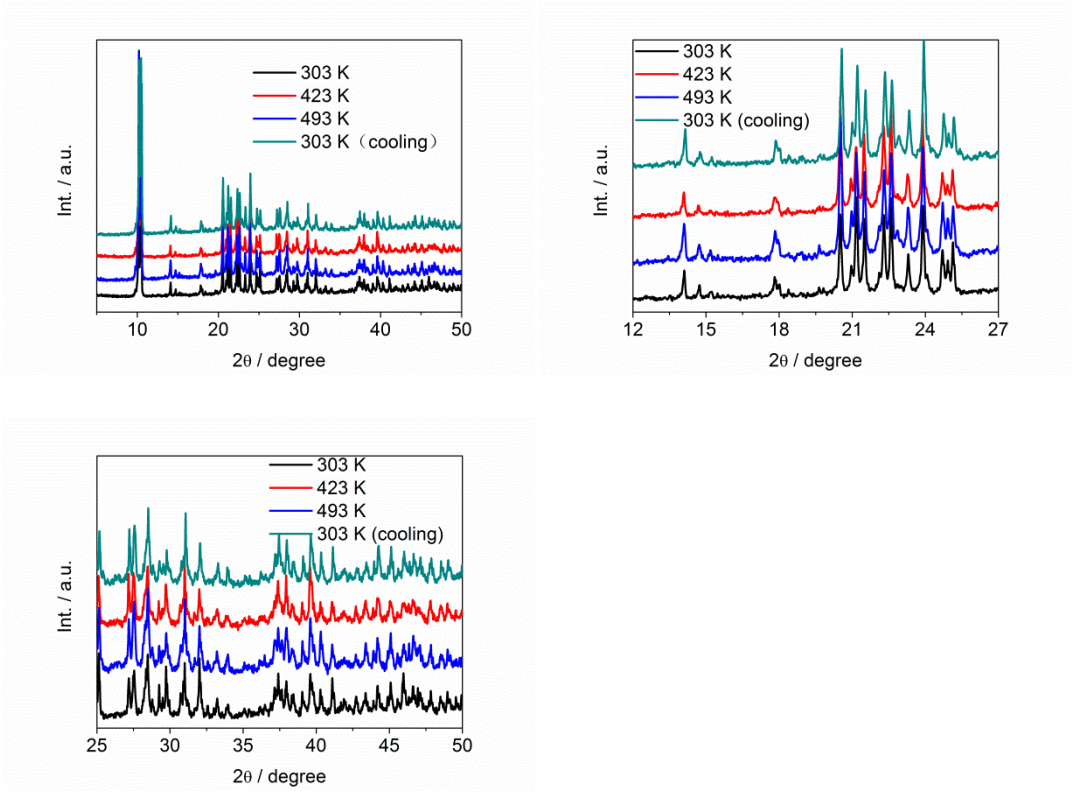

Fig. S17: Variable-temperature PXRD patterns of **1** in different 2θ ranges at 303 K (pristine sample), 423 and 493 K, 303 K (heated and cooled down).